Supplementary Material

Text S1 Materials and reagents

Zinc chloride dehydrate ($ZnCl_2$), Thioacetamide (TAA), Thiourea, Polyvinylpyrrolidone (PVP), triethanolamine (TEOA), Ascorbic acid (AA), Tert-butyl alcohol (TBA), and glycol were obtained from Sinopharm Chemical Reagent Co., Ltd (Beijing, China). P-benzoquinone (BQ), Bisphenol A (BPA), Resorcinol (RC), Sodium sulfate (Na_2SO_4) were acquired from Aladin Reagent Co., Ltd. (Shanghai, China). Indium nitrate tetrahydrate ($InCl_3 \cdot 4H_2O$) and Tetracycline (TC) were obtained from Macklin Biochemical Co., Ltd (Shanghai, China). Sodium dihydrate sodium molybdate ($Na_2MoO_4 \cdot 2H_2O$) was purchased from Tianjin Damao Chemical Plant (Tianjin, China). Absolute ethanol (EtOH), and Lactic acid were purchased from Fuyu Fine Chemical Co., Ltd (Tianjin, China). The Indium-Tin Oxides (ITO) were obtained from Zhuhai Kaivo Optoelectronic Technology Co., Ltd (Zhuhai, China). All other chemicals were of analytical reagent grade and used without further purification, deionized water was utilized in all experiments.

Text S2 Apparatus

The X-ray diffraction (XRD) patterns of the materials were obtained using a D8 advance X-ray diffractometer (Bruker AXS, Germany) with Cu *K*α radiation (λ =1.5406 A) at 40 kV and 40 mA. The morphology and crystal structure of the samples were studied by emission scanning electron microscope (SEM) (Quanta FEG 250, FEI, USA). The transmission electron microscopy (TEM) and high-resolution transmission electron microscopy (HRTEM) of the samples were obtained by transmission electron microscopy (JEM-2100F, JEOL, Japan). X-ray photoelectron spectroscopy (XPS) measurements were performed on a 2000 XPS system with a monochromatic Al Kα source and a charge neutralizer (Axis Supra, Kratos, Japan). UV-vis absorption spectra of the samples were recorded on a UV-vis spectrophotometer (Cary 500 Scan Spectrophotometers, Varian, USA) with a wavelength range of 200–800 nm. Surface area and porosity analysis were performed by nitrogen adsorption/desorption experiment using the BET method (ASAP2460, Micromeritics, USA). The photoluminescence (PL) spectra and fluorescence decay spectra were recorded on a Fluoro Max-4 spectrophotometer at room temperature (Fluoro Max-4, Horiba, USA).

Text S3 Photoelectrochemical measurements

The photoelectrochemical performances were measured in the CHI760E electrochemical analyzer (Chen Hua Instrument Co. Ltd., China) with a standard three electrode configuration. Under

visible light assembled by a 300W Xe lamp with a filter (λ > 420 nm). The modified ITO glass (2×1 cm), Pt plate and saturated calomel electrode (SCE) were employed as working electrode, counter electrode and reference electrode, respectively.

The transient photocurrent responses were tested in 0.1 mol/L Na_2SO_4 solution as electrolyte. EIS measurements were performed in 2.5 mmol/L $[Fe(CN)_6]^{3-/4-}$ (0.1 mol/L KCl) solution with a frequency range of 0.1–100 kHz at 0.24 V, and the amplitude of the applied sine wave potential in each case was 5 mV. The LSV curves were obtained with a mixed solution of 10% (v/v) lactic acid and 0.2 mol/L aqueous Na_2SO_4 solution. Moreover, Mott-Schottky (M-S) plots were carried out in the range of −1 to +1 V (vs. SCE) reference electrode under frequency of 1 kHz and 1.5 kHz in 0.2 mol/L Na_2SO_4 solution.

Text S4 Density Functional Theory (DFT)

The theoretical calculations were carried out using a Gaussian 09 package (Frisch and Trucks, 2009). The related structures were optimized by the DFT method at the B3LYP level with a standard 6-31G (d, p) basis set (Ma et al., 2017). All the optimized structures were confirmed to be stable because of no imaginary frequencies from the vibrational frequency calculations.

Equation S1 AQE equation

The AQE for H_2 production was measured under the same reaction conditions, only replacing the 420 nm cutoff filter with a band pass interference filter centered at 420, 450, 500, 550, and 600 nm, respectively. The AQE was obtained by the following Eq. (S1):

$$AQE = \frac{2 \times R_{H2}}{I} \times 100\% \qquad \text{(S1)}$$

Trapping experiments with quenchers were carried out to determine the main active species in pollutants degradation. triethanolamine (TEOA), tert-butyl alcohol (TBA) and p-benzoquinone (BQ) were used as h^+, ·OH, and $\cdot O_2^-$ radical quenchers, respectively.

Equation S2 Langmuir-Hinshelwood equation

Langmuir-Hinshelwood equation (Eq. (S2)):

$$r = \frac{kKC}{1 + KC} \qquad \text{(S2)}$$

where *r* is the initial HER rate (μmol/h), *k* is the HER rate constant (μmol/h), *K* is the adsorption constant (L/mg) and *C* is the initial BPA concentration (mg/L) (Lin et al., 2017). Here, the values of *k* and *K* are determined to be 4.35 μmol/h and 0.016 L/mg, respectively.

Equation S3 Adsorption experiments

The 15 mg adsorbent was added into 50 mL TC, RC, and BPA (50 mg/L). The adsorption kinetics experiments were carried out at 298K under stirring for 60 min. The mixtures were centrifuged at 10000 r/min and approximately 4 mL were taken from the suspension at predetermined times. The supernatant was transferred to a quartz cuvette for the absorbance measurement with a UV-vis-NIR spectrophotometer (Lamda 900, PerkinElmer, USA) to determine the concentration of organic pollutants.

The adsorption capacity q_e (mg/g) (Eq. (S3)) were calculated using the following formulas:

$$q_e = \frac{(C_0 - C_e)}{m} V \qquad \text{(S3)}$$

where C_0 (mg/L) and C_e (mg/L) are the concentration of TC, RC, and BPA before and after reaction, V (L) is the volume of the solution, m (g) is the dosage of adsorbent.

Equations S4 and S5 Decay lifetime equation

The decay process of the photocatalyst can be well fitted with a bi-exponential kinetic function as follows Eq. (S4) (Zhao et al., 2019):

$$I(t) = B_1 e^{-t} / \tau_1 + B_2 e^{-t} / \tau_2 \qquad \text{(S4)}$$

Equation (S5) shown below can be used to calculate the average lifetime τ of the photocatalyst (Zhang et al., 2017):

$$\tau = (B_1\tau_1^2 + B_2\tau_2^2) / (B_1\tau_1 + B_2\tau_2) \qquad \text{(S5)}$$

where τ_1/τ_2 represent lifetimes, B_1/B_2 represent pre-exponential factors and τ means the average lifetime of the carriers. As listed in Table S2, the average emission lifetime decreases from 2.84 ns for $ZnIn_2S_4$ to 4.57 ns for 10-OMS/ZIS, indicating the rapid electron transfer by OMS.

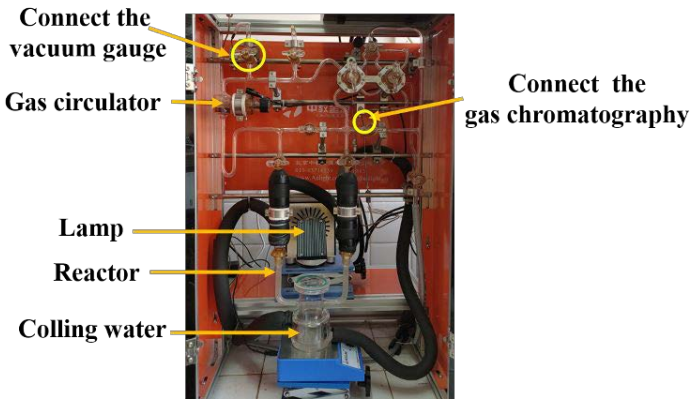

Fig. S1 Schematic diagram of the reaction set-up.

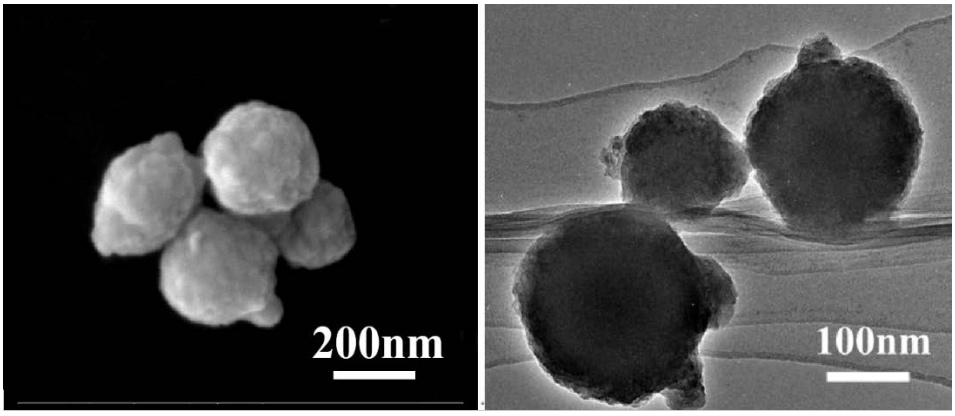

Fig. S2 SEM and TEM of the as-prepared OMS.

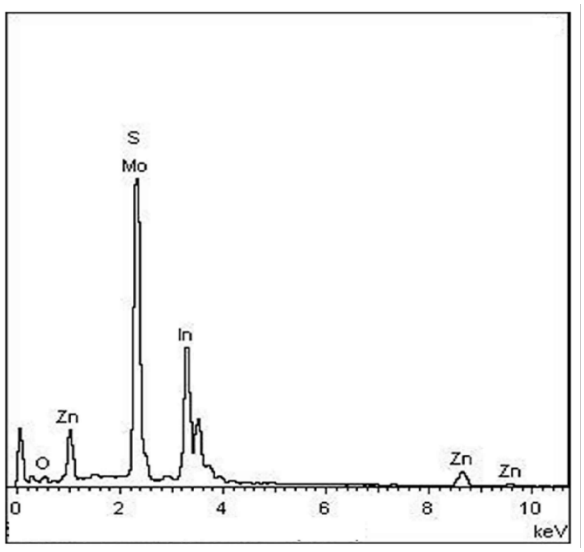

Fig. S3 EDS spectrum of 10-OMS/ZIS.

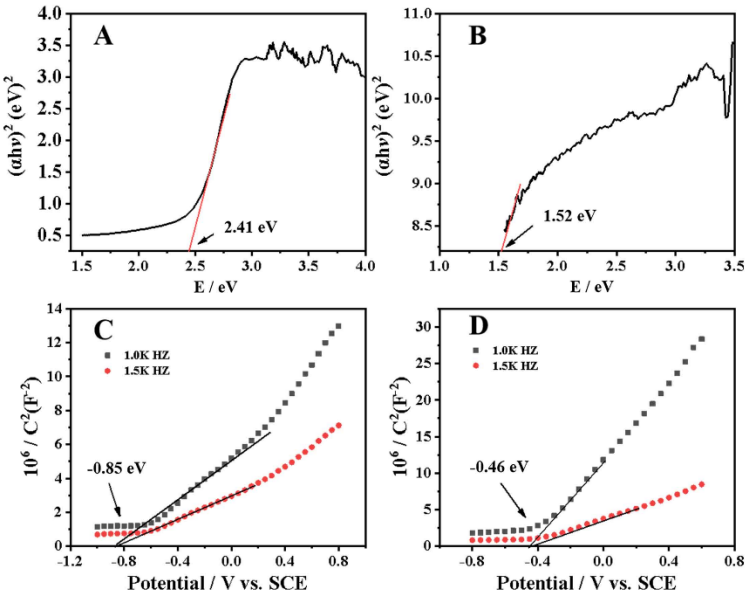

Fig. S4 (A)–(B) Band gap potential of $ZnIn_2S_4$ and OMS, (C)–(D) M-S curves of $ZnIn_2S_4$ and OMS.

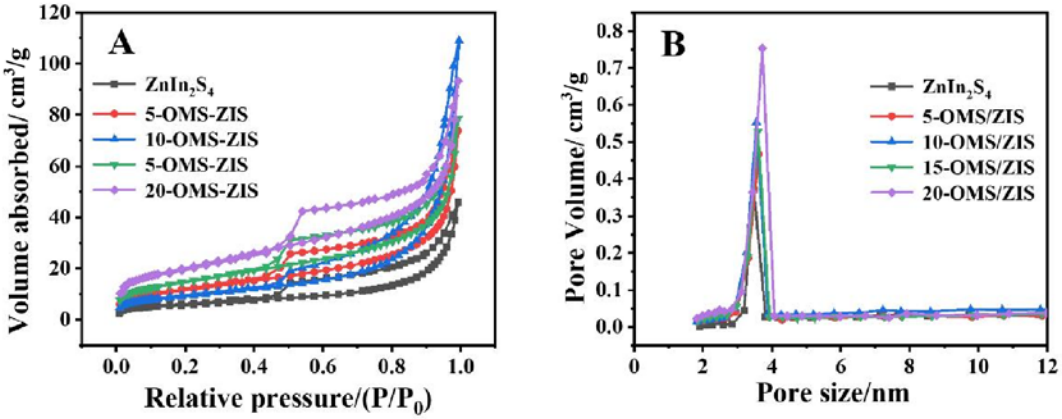

Fig. S5 N_2 adsorption-desorption isotherms (A), the Barrett-Joyner-Halenda (BJH) pore size distribution curve (B) of $ZnIn_2S_4$ and OMS/ZIS composite.

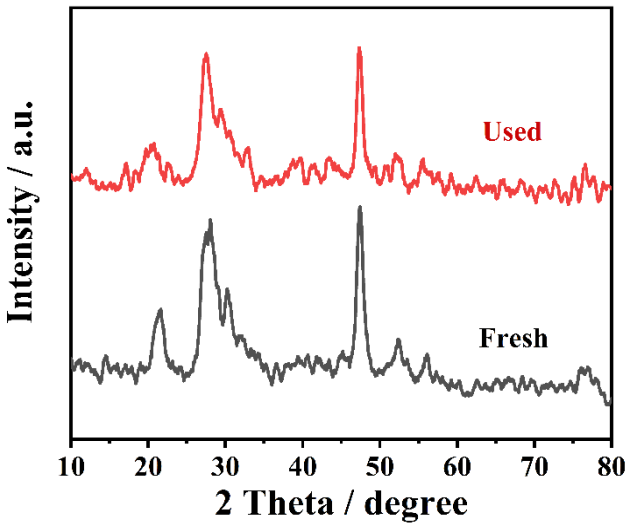

Fig. S6 XRD patterns of the fresh and used 10-OMS/ZIS.

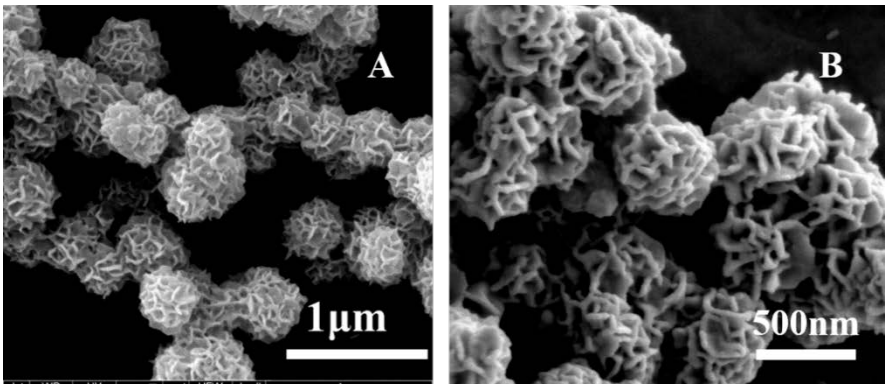

Fig. S7 SEM image of 10-OMS/ZIS (A) and after three cycles (B).

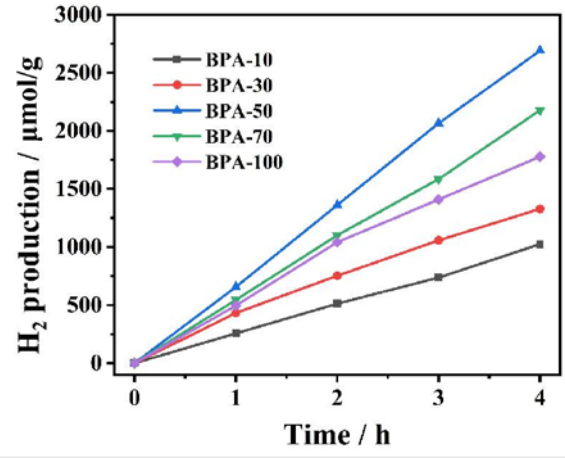

Fig. S8 Photocatalytic H_2 evolution rates over 10-OMS/ZIS with different concentration of BPA under visible light irradiation. Error bars show the standard deviation of repeated measurements (n = 3).

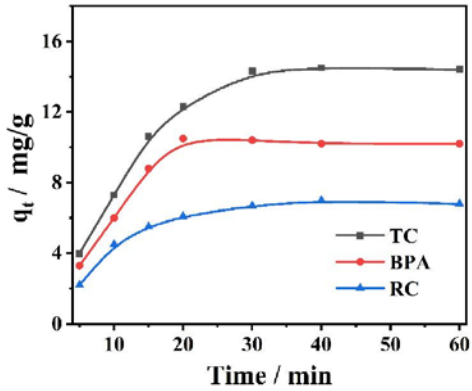

Fig. S9 Adsorption kinetic curves of TC, RC, and BPA. Error bars show the standard deviation of repeated measurements (n = 3).

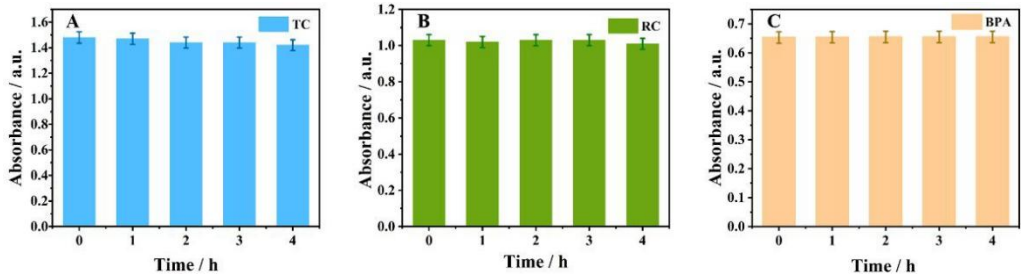

Fig. S10 The absorbance variation of TC (A), RC (B) and BPA (C) solution without photocatalyst. Error bars show the standard deviation of repeated measurements (n = 3).

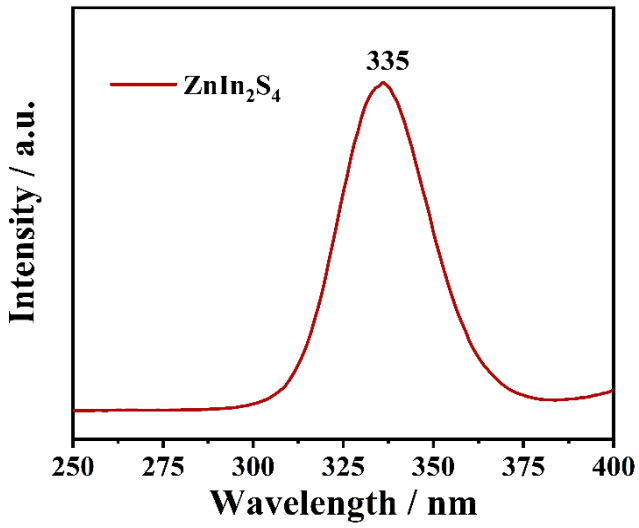

Fig. S11 Schematic illustration of excitation wavelength of $ZnIn_2S_4$.

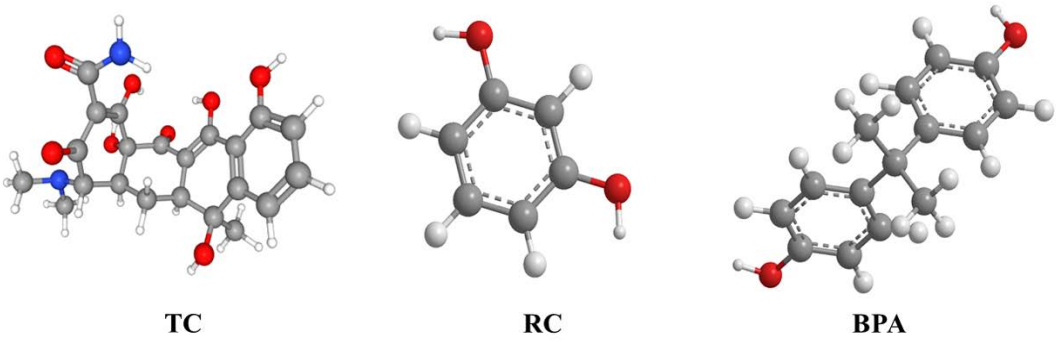

Fig. S12 The chemical structures of TC, RC, and BPA.

TC, RC, and BPA, as highly concerned organics in wastewater, were adopted as typical degradation target to further clarify the photocatalytic mechanism using organics as electron donors in the dual-functional system, due to the different redox potential, conjugated structure and charged properties.

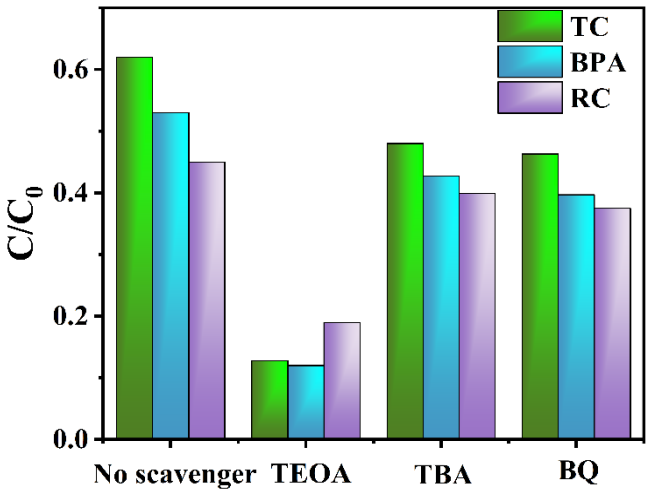

Fig. S13 Effects of scavengers on the photodegradation of TC, BPA, and RC. Error bars show the standard deviation of repeated measurements (n = 3).

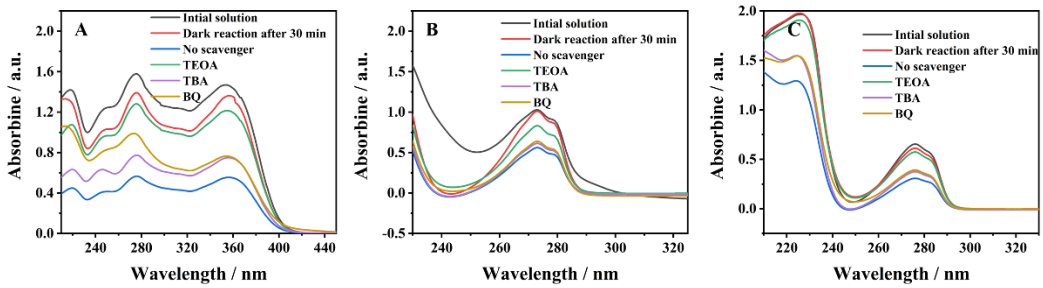

Fig. S14 Absorption spectra of TC (A), RC (B), and BPA (C) in trapping experiment.

Table S1 The BET surface area, pore size and pore volume of the materials.

Materials	BET Surface (m^2/g)	Pore Size (nm)	Pore volume (cm^3/g)
$ZnIn_2S_4$	19.1813	8.8983	0.0811
5-OMS/ZIS	42.0980	6.8600	0.1104
10-OMS/ZIS	52.2652	8.3071	0.1365
15-OMS/ZIS	53.0167	7.72261	0.1160
20-OMS/ZIS	72.6590	8.5458	0.1416

Table S2 Reported literatures of photocatalytic hydrogen evolution over the $MoS_2/ZnIn_2S_4$ composite.

Samples	Hydrogen production rate (μmol/g/h)	Condition: catalyst, Sacrificial agents, light	Source
OMS/ZIS	12800	15 mg 0.1 mol/L AA (ascorbic Acid) λ > 420 nm	this work
$ZnIn_2S_4/MoS_2$	3000	10 mg 10% LA (lactic acid) λ > 400 nm	(Lim et al., 2016)
$ZnIn_2S_4/MoS_2$	3060	50 mg 0.5 mol/L Na_2SO_3 and 0.43 mol/L Na_2S λ > 420 nm	(Wei et al., 2014)
$ZnIn_2S_4/MoS_2$ QDS	7000	20 mg 15% TEOA (triethanolamine) λ > 420 nm	(Liu et al., 2019)
2D/2D $ZnIn_2S_4/MoS_2$	5000	10% LA λ > 420 nm	(Huang et al., 2019)
MoS_2/CQDs/$ZnIn_2S_4$	3000	50 mg 10% TEOA λ > 420 nm	(Wang et al., 2018)
$MoS_2/ZnIn_2S_4$	3891.6	80 mg 0.25 mol/L Na_2SO_3 and 0.35 mol/L Na_2S λ > 420 nm	(Zhang et al., 2018)
$MoS_2/ZnIn_2S_4$	2512.5	80 mg 10% LA λ > 420 nm	(Liu et al., 2018)
2D $MoS_2/ZnIn_2S_4$	2910	25 mg 10% TEOA λ > 400 nm	(Li et al., 2017)
$MoS_2/ZnIn_2S_4$	4287.5	80 mg 10% LA λ > 420 nm	(Chai et al., 2017)
$MoS_2/ZnIn_2S_4$	975	80 mg 0.25 mol/L Na_2SO_3 and 0.35 mol/L Na_2S λ > 420 nm	(Tian et al., 2014)

Table S3 Fitted data summary of time-resolved fluorescence decay of the samples.

Samples	τ_1	B_1	τ_2	B_2	τ
$ZnIn_2S_4$	1.38	1071.6	6.7	84.1	2.84
10-OMS/ZIS	1.5	803.6	7.4	174	4.57

Table S4 Predicted HOMO, LUMO values of RC, TC and BPA using the B3LYP level with a standard 6-31G (d, p) basis set.

Name of pollutants	E_{HOMO} (eV)	E_{LUMO} (eV)	E_g (eV)
RC	−5.78	0.18	5.96
TC	−5.59	−1.61	3.97
BPA	−5.59	−0.07	5.52

References

Chai B, Liu C, Wang C, Yan J, Ren Z (2017). Photocatalytic hydrogen evolution activity over MoS2/ZnIn2S4 microspheres. Chinese Journal of Catalysis, 38(12): 2067–2075

Frisch M J, Trucks G W (2009). Gaussian 09 Revision A.02: Gaussian Inc., Wallingford CT. Wallingford, CT: Gaussian Inc.

Huang L, Han B, Huang X, Liang S, Deng Z, Chen W, Peng M, Deng H (2019). Ultrathin 2D/2D ZnIn2S4/MoS2 hybrids for boosted photocatalytic hydrogen evolution under visible light. Journal of Alloys and Compounds, 798: 553–559

Li W, Lin Z, Yang G (2017). A 2D self-assembled MoS2/ZnIn2S4 heterostructure for efficient photocatalytic hydrogen evolution. Nanoscale, 9(46): 18290–18298

Lim W Y, Hong M, Ho G W (2016). In situ photo-assisted deposition and photocatalysis of ZnIn2S4/transition metal chalcogenides for enhanced degradation and hydrogen evolution under visible light. Dalton Transactions (Cambridge, England : 2003), 45(2): 552–560

Lin Z, Li L, Yu L, Li W, Yang G (2017). Dual-functional photocatalysis for hydrogen evolution from industrial wastewaters. Physical Chemistry Chemical Physics, 19(12): 8356–8362

Liu C, Chai B, Wang C, Yan J, Ren Z (2018). Solvothermal fabrication of MoS2 anchored on ZnIn2S4 microspheres with boosted photocatalytic hydrogen evolution activity. International Journal of Hydrogen Energy, 43(14): 6977–6986

Liu Y, Li C F, Li X Y, Yu W B, Dong W D, Zhao H, Hu Z Y, Deng Z, Wang C, Wu S J, Chen H, Liu J, Wang Z, Chen L H, Li Y, Su B L (2019). Molybdenum disulfide quantum dots directing zinc indium sulfide heterostructures for enhanced visible light hydrogen production. Journal of Colloid and Interface Science, 551: 111–118

Ma J, Wang H, Liu X, Lu L, Nie L, Yang X, Chai Y, Yuan R (2017). Synthesis of tube shape MnO/C p composite from 3,4,9,10-perylenetetracarboxylic dianhydride for lithium ion batteries. Chemical Engineering Journal, 309: 545–551

Tian G, Chen Y, Ren Z, Tian C, Pan K, Zhou W, Wang J, Fu H (2014). Enhanced photocatalytic hydrogen evolution over hierarchical composites of ZnIn2 S4 nanosheets grown on MoS2 slices. Chemistry, an Asian Journal, 9(5): 1291–1297

Wang B, Deng Z, Fu X, Li Z (2018). MoS2/CQDs obtained by photoreduction for assembly of a ternary MoS2/CQDs/ZnIn2S4 nanocomposite for efficient photocatalytic hydrogen evolution under visible light. Journal of Materials Chemistry. A, Materials for Energy and Sustainability, 6(40): 19735–19742

Wei L, Chen Y, Lin Y, Wu H, Yuan R, Li Z (2014). MoS2 as non-noble-metal co-catalyst for photocatalytic hydrogen evolution over hexagonal ZnIn2S4 under visible light irradiations. Applied Catalysis B: Environmental, 144: 521–527

Zhang S, Wang L, Liu C, Luo J, Crittenden J, Liu X, Cai T, Yuan J, Pei Y, Liu Y (2017). Photocatalytic wastewater purification with simultaneous hydrogen production using MoS2 QD-decorated hierarchical assembly of ZnIn2S4 on reduced graphene oxide photocatalyst. Water Research, 121: 11–19

Zhang Z, Huang L, Zhang J, Wang F, Xie Y, Shang X, Gu Y, Zhao H, Wang X (2018). In situ constructing interfacial contact MoS2/ZnIn2S4 heterostructure for enhancing solar photocatalytic hydrogen evolution. Applied Catalysis B: Environmental, 233: 112–119

Zhao T, Xing Z, Xiu Z, Li Z, Yang S, Zhou W (2019). Oxygen-doped MoS2 nanospheres/CdS quantum dots/g-C3N4 nanosheets super-architectures for prolonged charge lifetime and enhanced visible-light-driven photocatalytic performance. ACS Applied Materials & Interfaces, 11(7): 7104–7111